PHOTONIC SENSORS / Vol. 12, No. 2, 2022: 140–151

Effect of PMMA Removal Methods on Opto-Mechanical Behaviors of Optical Fiber Resonant Sensor With Graphene Diaphragm

Yujian LIU[1], Cheng LI[1,2*], Shangchun FAN[1], and Xuefeng SONG[3]

[1]*School of Instrumentation Science and Opto-Electronics Engineering, Beihang University, Beijing 100191, China*

[2]*Research Institute of Beihang University in Shenzhen, Shenzhen 518057, China*

[3]*Shenzhen Institute for Quantum Science and Engineering, Southern University of Science and Technology, Shenzhen 518055, China*

[*]Corresponding author: Cheng LI E-mail: licheng@buaa.edu.cn

Abstract: Regarding the dependence of the treatment of removing polymethyl methacrylate (PMMA) from graphene upon the prestress in the film, two typical PMMA removal methods including acetone-vaporing and high-temperature annealing were investigated based on the opto-mechanical behaviors of the developed optical fiber Fabry-Perot (F-P) resonant sensor with a 125-μm diameter and ~10-layer-thickness graphene diaphragm. The measured resonant responses showed that the F-P sensor via annealing process exhibited the resonant frequency of 481 kHz and quality factor of 1 034 at ~2 Pa and room temperature, which are respectively 2.5 times and 33 times larger than the acetone-treated sensor. Moreover, the former achieved a high sensitivity of 110.4 kHz/kPa in the tested range of 2 Pa–2.5 kPa, apparently superior to the sensitivity of 16.2 kHz/kPa obtained in the latter. However, the time drift of resonant frequency also mostly tended to occur in the annealed sensor, thereby shedding light on the opto-mechanical characteristics of graphene-based F-P resonant sensors, along with an optimized optical excitation and detection scheme.

Keywords: Graphene diaphragm; PMMA removal; opto-mechanical behavior; F-P resonator

Citation: Yujian LIU, Cheng LI, Shangchun FAN, and Xuefeng SONG, "Effect of PMMA Removal Methods on Opto-Mechanical Behaviors of Optical Fiber Resonant Sensor with Graphene Diaphragm," *Photonic Sensors*, 2022, 12(2): 140–151.

1. Introduction

Graphene, a monolayer hexagonal lattice of carbon atoms, has demonstrated excellent mechanical [1], electrical [2], optical [3], and thermal properties [4]. Due to these superior properties, the research about the new material has expanded explosively in the field of micro-electro-mechanical systems (MEMS), such as high frequency transistors [5], surface plasmon resonant (SPR) devices [6–9], and mechanical resonators [10]. Note that graphene has the characteristics of ultra-thin thickness of 0.335 nm, high tensile rate up to 20% [11], and extreme fatigue life of more than 10^9 cycles [12]. These extraordinary properties make the material a suitable candidate as a sensitive and robust vibration element, especially as a competitively sensitive vibration diaphragm for nano-mechanical resonant sensors. Particularly, in 2007, Bunch *et al.* [10] fabricated the first graphene resonator by transferring graphene onto trenches and studied its natural frequency and quality factor.

Received: 23 February 2021 / Revised: 18 May 2021

DOI: 10.1007/s13320-021-0636-3
Article type: Regular

Afterwards, Bunch and co-workers transferred graphene onto a square groove so as to form a sealed cavity, and then the frequency of suspended graphene was observed to change with the ambient pressure [13], thus indicating the feasibility of graphene resonant pressure sensor. Then more efforts have been made to investigate the effects on resonance characteristics by changing the layer number, film shape, ambient temperature and pressure [14–16] or actuation-tuning methods [17, 18], along with the corresponding film vibration detection methods [10, 19]. For example, Chen *et al.* [20] demonstrated the temperature response of monolayer graphene resonators with a high Q factor of 10^4 at a temperature of 5 K. Then Barton *et al.* [21] fabricated multiple circular mechanical resonators with different film diameters, which showed a prominent improvement of Q factor with increasing sizes. It should be pointed out that Ma *et al.* [22] recently fabricated an optical fiber graphene resonator by transferring a multilayer graphene (MLG) onto a ferrule, which achieved a resonant frequency of 135 kHz and a Q factor of 81 in the vacuum pressure of 10^{-2} Pa at room temperature. It is worth mentioning that, compared with its electrical counterparts, optical excitation and detection scheme is a non-contact mechanism with higher measurement accuracy and better repeatability for suspended resonant structures [23, 24].

The aforementioned experimental investigations have significantly boosted the understanding of graphene resonance characteristics. However, in addition to the sensitive structure of resonator and environment condition, the film transferring-dependent fabrication scheme for a graphene resonator also limits the resonant performance due to the residue on graphene [25, 26]. As far as we know, the graphene transfer for micro-mechanical systems is now commonly realized with the help of polymers, such as the widely used polydimethylsiloxane (PDMS) and polymethyl methacrylate (PMMA) [27]. For the former, PDMS is durable, unreactive, moldable, resistant to many solvents, and of low surface free energy. After transferring the PDMS/graphene onto the target substrate, MLG tends to adhere to the substrate rather than the PDMS, thereby being released from PDMS and stamped onto the new substrate [28–30]. With this dry transfer scheme, MLG can be transferred on to a supported substrate. However, in certain circumstance where graphene is expected to be freestanding over the substrate, such as micro-trenches, the graphene transfer process using PDMS is not a good choice. Without the protection of the substrate, the removal of PDMS could cause the tearing of graphene. Alternatively, PMMA as a middle layer is developed. Unlike PDMS that maintains weak van der Waals force with graphene, PMMA coating forms covalent bonds with graphene. Furthermore, PMMA can be easily spin-coated on the graphene grown on the original substrate [31]. After transferring PMMA/graphene on to a desired substrate, PMMA coating can be removed by annealing over 300 ℃ [32] or washed off in acetone solution [33]. Unfortunately, certain PMMA residues would remain on the graphene surface [34], thus unavoidably affecting the vibration behaviors of graphene.

Therefore, in this paper, from the viewpoint of graphene-based resonant sensors, the acetone-vaporing and annealing treatment methods of the PMMA film were compared to examine the resonant characteristics of the developed graphene-based F-P resonators by using the methods described above. The experimental results revealed a strong correlation of resonant frequency and Q factor with PMMA residues because of the dominant interfacial strength change in graphene diaphragm. To be specific, with a better adhesion with the substrate and a higher inner-tension within the suspended diaphragm, the annealed MLG produces a fewer energy loss in one oscillation cycle with higher Q factor than the acetone-treated counterpart.

2. F-P sensor fabrication

Figure 1 illustrates the schematic diagram of the fabricated optical fiber F-P resonant sensor. At the beginning, the graphene diaphragm was prepared from a chemical vapor-deposited (CVD) ~10-layer commercial transfer graphene sample (ACS Material®, Nanjing XFNANO Materials Tech Co., Ltd., Nanjing, China), as shown in Fig. 1(a). The PMMA/MLG sample was further adhered onto a zirconia ferrule end face, whose inner diameter was 125 μm, with the aid of van der Waals force by a wet transfer process, as given in Figs. 1(b)–1(d). After that, the PMMA removal operations via acetone solution or thermal annealing treatment were used to remove the PMMA coating, as illustrated in Figs. 1(e1) and 1(e2), respectively. For the former, the PMMA/MLG-attached ferrule was placed in acetone vapor for 72 hours at room temperature to dissolve the PMMA on the MLG surface. Further, the ferrule was put in a drying oven for 30 minutes at a temperature of 60 ℃ to evaporate the residual moisture. For the latter, the ferrule attached with the PMMA/MLG film was baked in a vacuum furnace (10^{-2} Pa) at a certain high temperature. In order to analyze the temperature influence upon PMMA removal, three different temperatures (350 ℃, 400 ℃, and 440 ℃) were used to eliminate the PMMA coating. After that, a standard single mode fiber (SMF) was inserted into a ZrO_2 ferrule with an inner diameter of 125 μm, and the gap between the fiber end face and the MLG film formed an F-P cavity. This initial cavity length was controlled by a 1 μm resolution translation platform and confirmed by an optical spectrum analyzer (OSA) (AQ6370C, Yokogawa Electric Corporation, Tokyo, Japan). Then the SMF and the ferrule were bonded together with an epoxy adhesive (3M®). In this way, a simple and miniature micro-air-gap-based optical fiber F-P resonator covered with ~10 layer and 125 μm diameter MLG film was fabricated, shown in Fig. 1(f). The picture of the fabricated F-P resonator senor is depicted in Fig. 1(g). In this case, the opto-thermally excited F-P resonance for the developed resonant probe is available to estimate the applicability of different PMMA removal methods in graphene resonators.

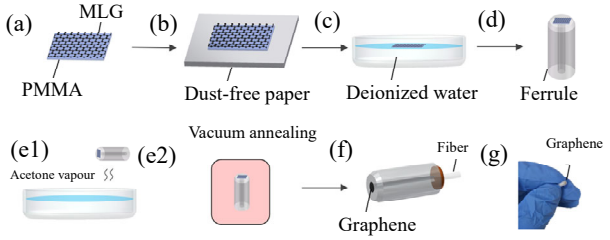

Fig. 1 Schematic diagram of graphene transfer process: (a) MLG on a PMMA substrate, (b) MLG/PMMA on a dust-free paper, (c) MLG/PMMA immersed in deionized water, (d) MLG/PMMA on a ferrule, (e1) MLG/PMMA dissolved in acetone vapour, (e2) MLG/PMMA annealed in a high-temperature furnace, (f) F-P resonant sensor with graphene diaphragm, and (g) picture of the fabricated F-P probe.

3. Experiment and result analysis

To study the opto-mechanical characteristics of graphene after PMMA removal process, the experimental setup for the optical excitation and detection scheme using the developed F-P resonant probe was established as shown in Fig. 2. A 1 550.12 nm amplitude-modulated distributed feedback (DFB) Laser 1 with an output power of 0.3 mW was utilized to generate a thermal excitation upon the circular graphene diaphragm with a diameter of 125 μm. The power of the Laser 1 was under the control of an electro-optic modulator (EOM) and a lock-in amplifier (HF2LI). Moreover, an erbium doped fiber amplifier (EDFA) was introduced to compensate the amplitude attenuation of the Laser 1 modulated by the EOM. Then, a 1 551.72 nm DFB Laser 2 with an output power of 3 mW was employed to detect the diaphragm vibration generated by periodically varying thermal stress. Thus, the two laser beams in charge of optical excitation and interrogation were optically coupled by a 2×1 coupler via a three-port circulator. The coupled signals were delivered to the F-P resonator and then irradiated to the surface of graphene diaphragm suspended on a capillary end face. The reflected light was collected by a photodetector (PD,

Beijing Conquer Optics Science & Technology Co., Ltd, Beijing, China) with a bandwidth of 200 MHz and a conversion gain of 1.4×10^4 V/W for observing and processing of useful F-P resonance signals. Note that the F-P resonance experiment was carried out in a vacuum chamber with adjustable ambient pressure ranging from 1 Pa to 10^5 Pa at room temperature.

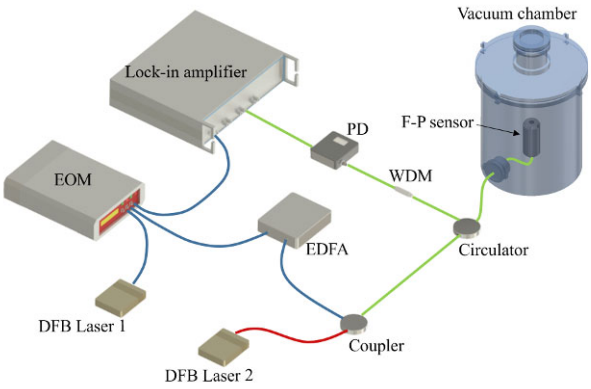

Fig. 2 Schematic diagram of fiber optic F-P resonant experimental setup.

3.1 Effect on MLG surface morphology

After the fabrication of the F-P resonant probe, the surface morphology of the suspended MLG was photographed, as illustrated in Fig. 3. Referring to Fig. 3(a), along with detectable PMMA residues, the folds were clearly observed on the MLG surface after acetone immersion and air-drying process, which is easy to cause a negative impact on the *Q* factor of F-P resonator due to non-uniformly distributed adsorbates or PMMA residues. In contrast, 350 ℃ thermally annealed suspended MLG surface in Fig. 3(b) revealed a better flatness and cleanliness, thereby indicating fewer PMMA residuals due to a lighter image contrast. However, the MLG that had been subjected to acetone vapour and then annealing process was badly damaged with obvious broken holes scattered on the 125 μm diameter diaphragm, as labelled in Fig. 3(c). This phenomenon possibly resulted from the thermal stress damage caused by unevenly distributed internal stress in graphene introduced by PMMA residues during acetone evaporating process.

Actually, during the temperature-rising process of annealing, PMMA would endure a glass transition while the inner-tension of PMMA started to rise [35]. With an increase in the temperature, the PMMA coating occurred to decompose in two stages, i.e., the first stage (at about 220 ℃) with the terminal C=C bonds of PMMA and the second stage with random C–C scission and predominant at a higher temperature (at about 300 ℃) [36]. In view of mechanical properties of PMMA, the hardness and elastic modulus of PMMA film showed a tendency of increase on account of the reduced chain length of the polymer and cross links of the polymer [37, 38]. After a 350 ℃ annealing, a thin PMMA coating remained on the surface of the diaphragm so as to provide the protection and support for the graphene diaphragm. The resulting strong covalent bond between graphene and PMMA enhanced the equivalent stiffness of the PMMA/MLG. Hence, the residual stress of PMMA on the graphene surface would produce an extra tension in graphene, accordingly enabling an increase in the resonant frequency of the graphene diaphragm.

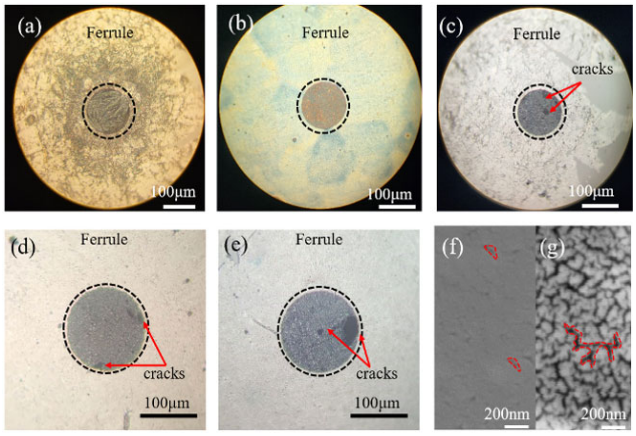

Fig. 3 Microscopy image of MLG on the ferrule treated by (a) acetone etching, (b) 350 ℃ annealing, (c) both acetone etching and annealing, (d) 400 ℃ annealing, and (e) 450 ℃ annealing. Note that graphene is marked inside the dotted line. The SEM images of (f) acetone treated MLG and (g) 350 ℃ annealed MLG, wherein the cracks are denoted by red dotted line.

Thermogravimetric (TG) curves can be utilized to describe the weight of PMMA residues as a

function of temperature. According to the TG curves in [39], the PMMA residues on the MLG surface would rapidly vanish when the temperature rose up to 400 ℃. Hence, higher temperatures (400 ℃ and 440 ℃) were tried in the PMMA/MLG annealing process. Although the remains of diaphragm showed an ultra-clean surface via an optical microscope, numerous cracks were still observed on the surface of the diaphragm so that the fabricated F-P resonators were unable to work in a stable resonant state. As shown in Figs. 3(d) and 3(e), the MLG diaphragm at higher temperatures indicated an extremely high rate of breakage (>95%). One possible explanation for the film breakage is that the folds or ripples on graphene formed during the growth and a cooling process had caused a part of graphene diaphragm to mechanically tear off when the PMMA coating was wiped off [40]. Another reason is partly due to the larger thermal interfacial interaction between the MLG and PMMA coating in the annealing process. In other words, the mismatch of the thermal expansion coefficient between the two materials would cause a bimetallic effect, therefore aggravating the damage of diaphragm. For example, when the F-P probe was heated, the ferrule substrate with a positive thermal expansive efficient would impose a tensile stress on the graphene with a negative thermal expansive efficient [41]. In contrast, when the probe was cooled, the suspended diaphragm was relaxed and then apt to behave a rougher morphology. According to the observed STM image in previous research [42], the suspended MLG without the support of a substrate tended to be easier to deform in the annealing treatment. Hence, it can be inferred from Figs. 3(a)–3(e) that the PMMA annealing treatment at 350 ℃, a relatively lower temperature, obtained a better smoothness of graphene diaphragm. Figures 3(f) and 3(g) further show SEM images (FEI Quanta 450) of the graphene surface after being treated by acetone and annealed at 350 ℃. Note that the number of flaws in Fig. 4(h) is much more than that in Fig. 4(f). Although there is no remarkable breakage on the annealed graphene diaphragm on a micron scale, in comparison with the previous work by Cheng [43], where such flaws did not appear on the graphene diaphragm with a diameter of 125 μm in the 350 ℃ annealing process, the cracks of tens nanometers were still available to be discerned, as denoted by red line in Fig. 3(g). The resulting phenomenon is primarily because that the area of the suspended diaphragm transferred onto the ferrule end-face is significantly larger than that in [43]. As a result, the larger graphene diaphragm without a support would be more vulnerable to the high temperature annealing process. It is important to note that the existence of micro-cracks has no major impact upon the following resonance experiment.

3.2 Effect on pressure-sensitive resonance response

Referring to Fig. 2 again, the sensors via acetone evaporating and annealing treatment, denoted by FRS 1 (F-P resonant sensor 1) and FRS 2 (F-P resonant sensor 2) correspondingly, were respectively placed in a vacuum chamber. The air pressure in the vacuum chamber was controlled to be ~2 Pa at the beginning, and then the vent valve of the chamber was unscrewed to let the outside air into the chamber. Meanwhile, the amplitude-frequency response was recorded during the rise of the pressure in the chamber. Figure 4 compares the measured resonance characteristics of the two resonators in the tested pressure range of 2 Pa–40 kPa. Then in this way, the relationship between the measured resonant response and the ambient pressure could be achieved based on the plotted three-dimensional image in Fig. 4.

It is well known that the resonant frequency and Q factor are the two key parameters for a resonant sensor. Moreover, the shift of resonant frequency reflects the response sensitivity to the ambient pressure. It can be concluded from Fig. (a) that the

resonant frequency of FRS 1 has increased by 71 kHz with the pressure ranging from 2 Pa to 33 kPa. For FRS 2, it showed a similar shift trend in frequency to FRS 1; however, the frequency shift was calculated to be as high as 279 kHz in the tested pressure range of 2 Pa to 40 kPa. Since the shift remained roughly unchanged after the pressure rose up to 2.5 kPa as shown in Fig. 4(b), therefore indicating a pressure sensitivity of 110.4 kHz/kPa in the effective range of 2 Pa to 2.5 kPa. Similarly, in Fig. 4(a), FRS 1 showed a pressure sensitivity of 16.3 kHz/kPa in the same pressure range. The measured sensitivity of 110.4 kHz/kPa is remarkably superior to those silicon or graphene-based resonant sensors (15 kHz/kPa and 90 kHz/kPa) in the previous work [44, 45].

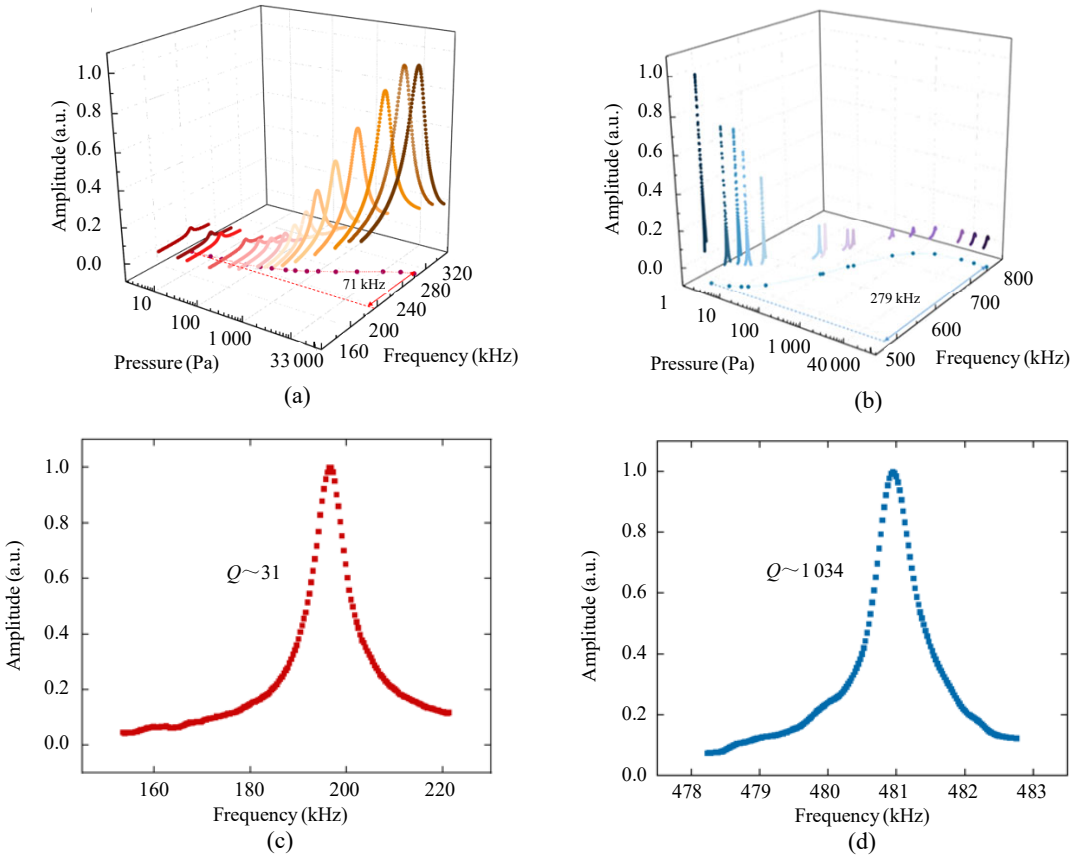

Fig. 4 Measured resonant amplitude-frequency response for (a) FRS 1 and (b) FRS 2 at various air pressures and for (c) FRS 1 and (d) FRS 2 at 2 Pa.

In terms of the monotone increasing frequency change with the pressure in the chamber, the sensor can be equivalent to a squeeze film model with regard to the existence of certain micro cracks on the graphene surface, as illustrated in aforementioned Fig. 3. In this case, if the air in the chamber is compressed at an extremely high frequency, the internal gas cannot escape owing to the viscous forces [46–48]. Thus, the added stiffness caused by the air compression turns out to be a function of pressure, thereby leading to a change of eigenfrequency. Hence, the resonant frequency of the diaphragm under pressure can be written as [45]

$$f^2 = f_0^2 + \frac{p}{4\pi^2 g_0 \rho} \tag{1}$$

where f and f_0 are the resonant frequencies of graphene at the ambient pressure p and vacuum pressure, respectively; g_0 is the gap size between the diaphragm and the substrate lying underneath, and ρ means the mass per unit square. It can be concluded

that the resonant frequency is positively correlated with the pressure. Furthermore, according to (1), the low mass density of graphene enables a super-high pressure sensitivity of this sensor. It can be also induced that the resonant frequency is the power function of pressure. In fact, as the pressure further increases, the air damping exerts a resistance on frequency variation. In this case, the resonant frequency tended to be stable when the pressure rose up to ~40 kPa, as denoted in Figs. 4(a) and 4(b). In particular, Knudsen number (K_n) can be introduced to estimate the air damping, which can be described as λ_{MFP}/l_{device}, where λ_{MFP} is the mean free path of air modules and l_{device} is the characteristic length of graphene device. As the pressure increases from 2 Pa to 40 kPa, K_n decreases from 4 to 2.5×10^{-4}, which means the flow state of air turns from the transition regime ($0.1<K_n<10$) to the continuum regime ($K_n<0.001$). Consequently, the rate of increase in frequency slowed down when the pressure rose up to 10^4 Pa, where $K_n=0.001$ means the critical point of continuum air flow regime.

The Q factor, as the energy loss in per oscillation circle, can be calculated by $\omega_0/\Delta\omega$, where ω_0 is the natural frequency and $\Delta\omega$ is the 3 dB bandwidth of the amplitude-frequency curve. The upper section of Fig. 5 shows the measured decreasing Q factors of FRS 1 and FRS 2 as a function of the pressure range of 2 Pa to ~40 kPa. It can be clearly found that FRS 2 obtained much better factors than FRS 1 as a whole. More specifically, the Q factors of FRS 2 were measured to be 1 034 and 632 at the pressures of ~2 Pa and 1 kPa, respectively, which were around 33.4 times and 45.1 times more than the results (31 and 14) of FRS 2. That is to say, the high-temperature annealing process is better than the acetone-treated method for a higher factor that means a more stable vibration and a stronger ability to resist external interference. In short, the fabricated annealed sensor behaves a relatively high quality factor and sensitivity. To better express the numerical characteristics of the developed sensor, the performance results of the typical graphene resonant pressure sensors are compared as listed in Table 1. Note that RT in Table 1 is short for room temperature.

Table 1 Performance comparison of graphene resonant pressure sensor.

Number	Layer number	Film shape	Side length/ diameter (μm)	Exciting method	Detection method	Resonant frequency	Quality factor (RT)	Pressure sensitivity (kHz/kPa)	Ref.
1	1–75 layers	Square	4.75	Optical	Optical	30 MHz–90 MHz	~25	-	[13]
2	Multilayer	Circle	125	Optical	Optical	60 kHz–240 kHz	81–103	-	[22]
3	Few-layer	Circle	5	Optical	Optical	~12 MHz	100	90	[45]
4	10 layers	Circle	125	Optical	Optical	481 kHz–760 kHz	1 034	110.4	This work

According to the previous literatures [49], Q factor can be described as

$$\frac{1}{Q}=\frac{1}{Q_a}+\frac{1}{Q_s}+\frac{1}{Q_i} \tag{2}$$

where $1/Q_a$, $1/Q_s$, and $1/Q_i$ represent the energy losses in surrounding environment, in the coupling of the resonator and the supporting substrate, and in the material, respectively.

For the developed FRS 1 and FRS 2 with multilayer graphene diaphragm, the air damping-dependent value of $1/Q_a$ should be nearly equal due to the same experimental conditions. In this case, the Q factor mainly depends on the latter two items in (2). As illustrated in [43], for a single layer graphene on a silicon oxide substrate, the average height h and the root-mean-square (rms) of surface roughness R_a of graphene sheet were measured to be 1.5 nm and 0.54 nm, respectively. After an annealing process of 400 °C,

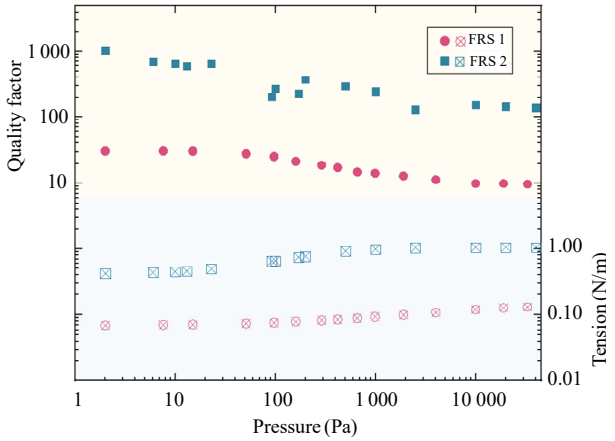

Fig. 5 Upper section: measured Q factor of the acetone-treated and annealed resonant sensors as a function of air pressure. Lower section: calculated diaphragm tension of graphene for FRS 1 and FRS 2 at different pressures.

h and R_a then behaved a reduction of 73.3% and 72.2%, which indicated a closer distance between graphene and silicon oxide, i.e., a flatter diaphragm surface. In fact, when the used multilayer graphene was transferred onto the substrate, wrinkles and contaminant polymers on graphene would hinder a perfect adhesion between the graphene diaphragm and the substrate. However, these contaminant polymers could be decomposed while being heated at an appropriate temperature. Thus, the interfacial contact between the substrate and the diaphragm can be further optimized so as to achieve a better interfacial adhesion and then less energy loss in a vibration cycle of resonator. This also explains the reason why the value of $1/Q_s$ of FRS 2 is lower than that of FRS 1.

In reality, Oshidari *et al.* [50] ever fabricated graphene resonators on a trench of SU-8 substrate by employing the 600 ℃ thermal treatment, wherein the shrinkage of SU-8 trench produced an extra tensile stress in graphene beam, thereby leading to an extremely high Q factor of more than 7 000 in one of the fabricated graphene resonators. It is important to note that the annealing temperature in [50] is far above the temperature in our experimental setup. That is due to the small size of the device (~5 μm) which is conducive for graphene to support itself and greatly reduces the risk of damage. Hence, the unnecessary energy loss in vibration can be avoided by increasing the internal tension in the graphene diaphragm [51]. In this way, with regard to the energy loss in graphene membrane ($1/Q_i$), the diaphragm tension of the vibrating graphene can be approximately given by [52]

$$S=\frac{r^2\rho l}{0.146}\left[f_{\text{air}}^2\cdot\left(1+\frac{\rho_{\text{air}}r\Gamma}{\rho l}\right)-\frac{0.22El^2}{\rho(1-\nu^2)r^4}\right] \quad (3)$$

where f_{air} is the resonant frequency in air; ρ and ρ_{air} are the mass densities of graphene and air; r, S, E, l, and ν are the radius, tension, Young's modulus, thickness, and Poisson's ratio of graphene, respectively [53, 54]. Note that Γ is a non-dimensionalized added virtual mass incremental factor as a function of mode shapes and boundary conditions, and Γ=0.746 in the fundamental resonant mode $f_{0,1}$. In this way, the diaphragm tension of graphene for the fabricated F-P resonators is shown in the bottom half of Fig. 5. A lower diaphragm tension represents a smaller film stiffness, corresponding to a possible high vibration amplitude. In generally, the diaphragm tension of graphene for FRS 1 showed a minimum S value of 0.07 N/m and a fluctuation of less than 2.7 dB in the tested pressure range, which was obviously smaller than that for FRS 2 with a fluctuation of approximately 4.0 dB and a minimum S value of 0.42 N/m. Furthermore, the difference in diaphragm tension for the two PMMA removal methods to a certain extent showed that the graphene-PMMA interfacial interaction induced by the annealing treatment was more sensitive to the pressure change with a more outstanding pressure sensitivity as well as the pressure measurement range. In other words, the graphene sensor fabricated by the acetone-vaporing treatment is more suitable for a limited measurement range with a high sensitivity. In addition, in combination with the two halves of Fig. 5, higher air

damping and diaphragm tension further reduced the Q factor at the pressure above 1 kPa. Also, the flaws on the diaphragm caused unnecessary energy loss due to the atom collision within the graphene harmonic vibrator.

3.3 Effect on stability of resonant frequency

Frequency stability is another important parameter for an applicable resonant sensor. Figure 6 compares the short-term time drift of resonant frequency within 15 minutes for FRS 1 and FRS 2 at a vacuum pressure of ~2 Pa. It can be observed from Fig. 6 that FRS 1 behaved a frequency increase of 1.0 kHz in 15 minutes with an average frequency drift of about 0.067 kHz/min. However, this increase accounts for negligible less than 0.5% with regard to the initial frequency of 199.12 kHz. By contrast, for FRS 2, its resonant frequency drifted with a larger average frequency change of ~1.48 kHz/min, which was 22 times higher than that for FRS 1. With respect to the beginning value of 470.75 kHz, the relatively high frequency change rate of FRS 2 (3.4%) was primarily due to the vibration instability of diaphragm that was concerned with certain micro-flaws generated by the annealing process. In order to further clarify the problem, the surface morphology image of the graphene diaphragm suspended on the two F-P resonators was monitored via a microscope, as presented in the inset in Fig. 6. From the inset of FRS 2 in Fig. 6, a little central hole with a diameter of around 10 μm appeared in the center of the annealed MLG after 15 minutes of optical excitation, which was marked in the red circle. The size of the defect hole would gradually spread with the continuous irradiation of laser as time went on. Then the effective optical reflection surface area would gradually decrease so as to accordingly result in the reduced reflected optical intensity. Along with the occurrence and then enlargement of a defect hole, the gas passage tended to be established at both sides of graphene diaphragm adhered on the ferrule end-face. As a consequence, the air pressure in the vacuum chamber approached to increase, therefore to some extent degree leading to a slightly larger resonant frequency.

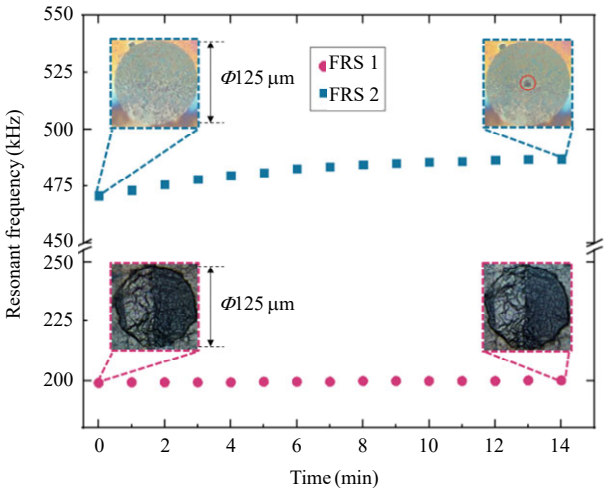

Fig. 6 Time drifts of the resonant frequency for FRS 1 and FRS 2 at ~2 Pa.

It should be clarified that there is a threshold in the power of laser that has an influence on the stability of graphene resonator. For instance, when the probe and pump lasers were respectively set as the higher laser powers of 5 mW and 0.5 mW, the developed resonator behaved a rather unstable vibration state, and the suspended graphene sheet would even be burned through in 90 seconds. Thus, to decrease the damage caused by the laser with a high power output, the output laser power was reduced by 40% with the corresponding powers of 3 mW and 0.3 mW for the probe laser and pump laser. However, it is worth mentioning that a reduction of laser power would lead to a weaker reflected signal power, thereby resulting in a lower SNR.

4. Conclusions

Optical fiber F-P resonant sensors with multilayer graphene diaphragm were fabricated to examine the effect of both acetone-vaporing and high-temperature annealing treatments on opto-mechanical response of graphene by optical excitation and detection. Compared with the

acetone-vaporing method, the annealing process strengthened the diaphragm stiffness in addition to reduced PMMA residues with a cleaner diaphragm surface, thus significantly improving the resonant frequency and Q factor of graphene resonator. Hence, the annealed F-P sensor demonstrated a resonant frequency of 481 kHz and Q factor of 1 034 at ~2 Pa and room temperature, which are approximately 2.5 times and 33 times higher than that of the sensor treated by the acetone method. Furthermore, the former behaved a high pressure sensitivity of 110.4 kHz/kPa in the pressure range of 2 Pa–2.5 kPa, which is outstandingly 6.8 times higher than the latter. Unfortunately, the annealing process would negatively weaken the mechanical strength of diaphragm itself, such that the annealed diaphragm was found to be more easily broken under a long-time harmonic excitation of laser with a high output power. In particular, the resonant frequency of the annealed resonator presented a more obvious time drift due to an irreversible film damage caused by continuous photothermal expansion and contraction. Therefore, in combination with optimized optical excitation and detection parameters of laser, appropriate PMMA removal methods contribute to the fabrication of high-performance graphene-based optical resonators.

Acknowledgment

This work was supported by the National Natural Science Foundation of China (Grant Nos. 61573033 and 61773045), the National Defense Science and Technology Innovation Zone, Beijing Natural Science Foundation (Grant No. 4212039), and Science Technology and Innovation Commission of Shenzhen Municipality (Grant Nos. JCYJ20180504165721952 and JCYJ-20170817-111857745), and Aviation Science Foundation of China (Grant No. 2020Z073051002).

References

[1] C. Lee, X. Wei, J. W. Kysar, and J. Hone, "Measurement of the elastic properties and intrinsic strength of monolayer graphene," *Science*, 2008, 321(5887): 385–388.

[2] J. Sakamoto, J. van Heijst, O. Lukin, and A. D. Schlüter, "Two-dimensional polymers: just a dream of synthetic chemists," *Angewandte Chemie International Edition*, 2009, 48(6): 1030–1069.

[3] F. Bonaccorso, Z. Sun, T. A. Hasan, and A. C. Ferrari, "Graphene photonics and optoelectronics," *Nature Photonics*, 2010, 4(9): 611–622.

[4] A. A. Balandin, S. Ghosh, W. Bao, I. Calizo, D. Teweldebrhan, F. Miao, *et al.*, "Superior thermal conductivity of single-layer graphene," *Nano Letters*, 2008, 8(3): 902–907.

[5] A. Das, S. Pisana, B. Chakraborty, S. Piscanec, S. K. Saha, U. V. Waghmare, *et al.*, "Monitoring dopants by Raman scattering in an electrochemically top-gated graphene transistor," *Nature Nanotechnology*, 2008, 3(4): 210–215.

[6] C. Cen, Y. Zhang, X. Chen, H. Yang, Z. Yi, W. Yao, *et al.*, "A dual-band metamaterial absorber for graphene surface plasmon resonance at terahertz frequency," *Physica E: Low-dimensional Systems and Nanostructures*, 2020, 117: 113840.

[7] L. Jiang, C. Yuan, Z. Li, J. Su, Z. Yi, W. Yao, *et al.*, "Multi-band and high-sensitivity perfect absorber based on monolayer graphene metamaterial," *Diamond and Related Materials*, 2021, 111(1): 108227.

[8] Z. Chen, H. Chen, H. Jile, D. Xu, Z. Yi, Y. Lei, *et al.*, "Multi-band multi-tunable perfect plasmon absorber based on L-shaped and double-elliptical graphene stacks," *Diamond and Related Materials*, 2021, 115: 108374.

[9] Z. He, L. Li, H. Ma, L. Pu, H. Xu, Z. Yi, *et al.*, "Graphene-based metasurface sensing applications in terahertz band," *Results in Physics*, 2021, 21: 103795.

[10] J. S. Bunch, A. M. van der Zande, S. S. Verbridge, I. W. Frank, D. M. Tanenbaum, J. M. Parpia, *et al.*, "Electromechanical resonators from graphene sheets," *Science*, 2007, 315(5811): 490–493.

[11] J. W. Jiang, J. S. Wang, and B. Li, "Young's modulus of graphene: a molecular dynamics study," *Physical Review B*, 2009, 80(11): 113405.

[12] T. Cui, S. Mukherjee, P. M. Sudeep, G. Colas, F. Najafi, J. Tam, *et al.*, "Fatigue of graphene," *Nature*

Materials, 2020, 19(4): 405–411.
[13] J. S. Bunch, S. S. Verbridge, J. S. Alden, A. M. van der Zande, J. M. Parpia, H. G. Craighead, *et al*., "Impermeable atomic membranes from graphene sheets," *Nano Letters*, 2008, 8(8): 2458–2462.
[14] V. Singh, S. Sengupta, H. S Solanki, R. Dhall, A. Allain, S. Dhara, *et al.*, "Probing thermal expansion of graphene and modal dispersion at low-temperature using graphene nanoelectro-mechanical systems resonators," *Nanotechnology*, 2010, 21(16): 165204.
[15] A. M. van der Zande, R. A. Barton, J. S. Alden, C. S. Ruiz-Vargas, W. S. Whitney, P. H. Q. Pham, *et al.*, "Large-scale arrays of single-layer graphene resonators," *Nano Letters*, 2010, 10(12): 4869–4873.
[16] D. Miller and B. Alemán, "Shape tailoring to enhance and tune the properties of graphene nanomechanical resonators," *2D Materials*, 2017, 4(2): 025101.
[17] X. Song, M. Oksanen, M. A. Sillanpää, H. G. Craighead, J. M. Parpia, and P. J. Hakonen, "Stamp transferred suspended graphene mechanical resonators for radio frequency electrical readout," *Nano Letters*, 2012, 12(1): 198–202.
[18] F. Guan, P. Kumaravadivel, D. V. Averin, and X. Du, "Tuning strain in flexible graphene nano-electromechanical resonators," *Applied Physics Letters*, 2015, 107(19): 193102.
[19] D. Garcia-Sanchez, A. M. van der Zande, A. S. Paulo, B. Lassagne, P. L. McEuen, and A. Bachtold, "Imaging mechanical vibrations in suspended graphene sheets," *Nano Letters*, 2008, 8(5): 1399–1403.
[20] C. Chen, S. Rosenblatt, K. I. Bolotin, W. Kalb, P. Kim, I. Kymissis, *et al.*, "Performance of monolayer graphene nanomechanical resonators with electrical readout," *Nature Nanotechnology*, 2009, 4(12): 861–867.
[21] R. A. Barton, B. Ilic, A. M. van der Zande, W. S. Whitney, P. L. McEuen, J. M. Parpia, *et al*., "High, size-dependent quality factor in an array of graphene mechanical resonators," *Nano Letters*, 2011, 11(3): 1232–1236.
[22] J. Ma, W. Jin, H. Xuan, C. Wang, and H. L. Ho, "Fiber-optic ferrule-top nanomechanical resonator with multilayer graphene film," *Optics Letters*, 2014, 39(16): 4769–4772.
[23] T. Larsen, S. Schmid, L. G. Villanueva, and A. Boisen, "Photothermal analysis of individual nanoparticulate samples using micromechanical resonators," *ACS Nano*, 2013, 7(7): 6188–6193.
[24] D. Ramos, O. Malvar, Z. J. Davis, J. Tamayo, and M. Calleja, "Nanomechanical plasmon spectroscopy of single gold nanoparticles," *Nano Letters*, 2018, 18(11): 7165–7170.
[25] M. Her, R. Beams, and L. Novotny, "Graphene transfer with reduced residue," *Physics Letters A*, 2013, 377(21–22): 1455–1458.
[26] X. Liang, B. A. Sperling, I. Calizo, G. Cheng, C. A. Hacker, Q. Zhang, *et al.*, "Toward clean and crackless transfer of graphene," *ACS Nano*, 2011, 5(11): 9144–9153.
[27] J. Kang, D. Shin, S. Bae, and B. H. Hong, "Graphene transfer: key for applications," *Nanoscale*, 2012, 4(18): 5527–5537.
[28] K. S. Kim, Y. Zhao, H. Jang, S. Y. Lee, J. M. Kim, K. S. Kim, *et al.*, "Large-scale pattern growth of graphene films for stretchable transparent electrodes," *Nature*, 2009, 457(7230): 706–710.
[29] S. J. Kang, B. Kim, K. S. Kim, Y. Zhao, Z. Chen, G. H. Lee, *et al.*, "Inking elastomeric stamps with micro-patterned, single layer graphene to create high-performance OFETs," *Advanced Materials*, 2011, 23(31): 3531–3535.
[30] S. Cha, M. Cha, S. Lee, J. H. Kang, and C. Kim, "Low-temperature, dry transfer-printing of a patterned graphene monolayer," *Scientific Reports*, 2015, 5(1): 17877.
[31] U. Ali, K. J. B. A. Karim, and N. A. Buang, "A review of the properties and applications of Poly (Methyl Methacrylate) (PMMA)," *Polymer Reviews*, 2015, 55(4): 678–705.
[32] A. Reina, X. Jia, J. Ho, D. Nezich, H. Son, V. Bulovic, *et al.*, "Large area, few-layer graphene films on arbitrary substrates by chemical vapor deposition," *Nano Letters*, 2009, 9(1): 30–35.
[33] S. Schmid, T. Bagci, E. Zeuthen, J. M. Taylor, P. K. Herring, M. C. Cassidy, *et al.*, "Single-layer graphene on silicon nitride micromembrane resonators," *Journal of Applied Physics*, 2014, 115(5): 054513.
[34] G. B. Barin, Y. Song, I. F. Gimenez, A. G. S. Filho, L. S. Barreto, and J. Kong, "Optimized graphene transfer: influence of polymethylmethacrylate (PMMA) layer concentration and baking time on graphene final performance," *Carbon*, 2015, 84: 82–90.
[35] D. Mathiesen, D. Vogtmann, and R. B. Dupaix, "Characterization and constitutive modeling of stress-relaxation behavior of Poly (methyl methacrylate) (PMMA) across the glass transition temperature," *Mechanics of Materials*, 2014, 71: 74–84.
[36] W. R. Zeng, S. F. Li, and W. K. Chow, "Review on chemical reactions of burning Poly (methyl methacrylate) PMMA," *Journal of Fire Sciences*, 2002, 20(5): 401–433.
[37] E. Süske, T. Scharf, P. Schaaf, E. Panchenko, D. Nelke, M. Buback, *et al.*, "Variation of the mechanical properties of pulsed laser deposited PMMA films during annealing," *Applied Physics A*, 2004, 79(4): 1295–1297.

[38] Y. Nanzai, A. Miwa, and S. Z. Cui, "Aging in fully annealed and subsequently strained Poly (methyl methacrylate)," *Polymer Journal*, 2000, 32(1): 51–56.

[39] M. Ferriol, A. Gentilhomme, M. Cochez, N. Oget, and J. L. Mieloszynski, "Thermal degradation of Poly (methyl methacrylate) (PMMA): modelling of DTG and TG curves," *Polymer Degradation and Stability*, 2003, 79(2): 271–281.

[40] X. Li, W. Cai, J. An, S. Kim, J. Nah, D. Yang, *et al.*, "Large-area synthesis of high-quality and uniform graphene films on copper foils," *Science*, 2009, 324(5932): 1312–1314.

[41] W. Bao, F. Miao, Z. Chen, H. Zhang, W. Jang, C. Dames, *et al.*, "Controlled ripple texturing of suspended graphene and ultrathin graphite membranes," *Nature Nanotechnology*, 2009, 4(9): 562–566.

[42] S. Ryu, L. Liu, S. Berciaud, Y. J. Yu, H. Liu, P. Kim, *et al*., "Atmospheric oxygen binding and hole doping in deformed graphene on a SiO_2 substrate," *Nano Letters*, 2010, 10(12): 4944–4951.

[43] Z. Cheng, Q. Zhou, C. Wang, Q. Li, C. Wang, and Y. Fang, "Toward intrinsic graphene surfaces: a systematic study on thermal annealing and wet-chemical treatment of SiO_2-supported graphene devices," *Nano Letters*, 2011, 11(2): 767–771.

[44] D. R. Southwortha, H. G. Craighead, and J. M. Parpia, "Pressure dependent resonant frequency of micromechanical drumhead resonators," *Applied Physics Letters*, 2009, 94(21): 213506.

[45] R. J. Dolleman, D. Davidovikj, S. J. Cartamil-Bueno, H. S. J. van der Zant, and P. G. Steeneken, "Graphene squeeze-film pressure sensor," *Nano Letters*, 2016, 16(1): 568–571.

[46] M. K. Andrews, G. C. Turner, P. D. Harris, and I. M. Harris, "A resonant pressure sensor based on a squeezed film of gas," *Sensors and Actuators A: Physical*, 1993, 36(3): 219–226.

[47] M. Bao and H. Yang, "Squeeze film air damping in MEMS," *Sensors and Actuators A: Physical*, 2007, 136(1): 3–27.

[48] S. S. Rao, "*Vibration of continuous systems*," New Jersey: John Wiley & Sons, 2007.

[49] G. Feng, "*Theory and devices of resonant sensing*," Beijing: Tsinghua University Press, 2008.

[50] Y. Oshidari, T. Hatakeyama, R. Kometani, S. Warisawa, and S. Ishihara, "High-quality factor graphene resonator fabrication using resist shrinkage-induced strain," *Applied Physics Express*, 2012, 5(11): 117201.

[51] M. Olfatnia, T. Xu, L. S. Ong, J. M. Miao, and Z. H. Wang, "Investigation of residual stress and its effects on the vibrational characteristics of piezoelectric-based multilayered micro-diaphragms," *Journal of Micromechanics and Microengineering*, 2009, 20(1): 015007.

[52] A. Castellanos-Gomez, R. van Leeuwen, M. Buscema, H. S. J. van der Zant, G. A. Steele, and W. J. Venstra, "Single-layer MoS_2 mechanical resonators," *Advanced Materials*, 2013, 25(46): 6719–6723.

[53] C. Li, T. Lan, X. Yu, N. Bo, J. Dong, and S. Fan, "Room-temperature pressure-induced optically-actuated Fabry-Perot nanomechanical resonator with multilayer graphene diaphragm in air," *Nanomaterials*, 2017, 7(11): 366.

[54] M. K. Kwak, "Vibration of circular plates in contact with water," *Journal of Applied Mechanics*, 1991, 58(2): 480–483.